JGR Solid Earth

RESEARCH ARTICLE
10.1029/2020JB019936

Along-Dip Variation in Seismic Radiation of the 2011 Ibaraki-Oki, Japan, Earthquake (M_w 7.9) Inferred Using a Multiple-Period-Band Source Inversion Approach

Hisahiko Kubo[1], Kimiyuki Asano[2], Tomotaka Iwata[2], and Shin Aoi[1]

[1]National Research Institute for Earth Science and Disaster Resilience, Tsukuba, Japan, [2]Disaster Prevention Research Institute, Kyoto University, Uji, Japan

Key Points:
- The source models for the 2011 Ibaraki-oki earthquake were estimated in three successive period bands (5–10, 10–25, and 25–50 s) from near-source waveforms
- Short-period (5–10 s) and long-period (10–25 and 25–50 s) seismic waves were predominantly radiated from different regions along the dip direction during this event
- This along-dip variation in period-dependent seismic radiation is consistent with the idea that the scale in unstable sliding patches varies with depth

Supporting Information:
- Supporting Information S1

Correspondence to:
H. Kubo,
hkubo@bosai.go.jp

Citation:
Kubo, H., Asano, K., Iwata, T., & Aoi, S. (2020). Along-dip variation in seismic radiation of the 2011 Ibaraki-oki, Japan, earthquake (M_w 7.9) inferred using a multiple-period-band source inversion approach. *Journal of Geophysical Research: Solid Earth*, *125*, e2020JB019936. https://doi.org/10.1029/2020JB019936

Received 8 APR 2020
Accepted 17 SEP 2020
Accepted article online 21 SEP 2020

Abstract To elucidate the spatial variation in period-dependent seismic radiation for the 2011 Ibaraki-oki earthquake (M_w 7.9) in Japan, we applied a multiple-period-band source inversion approach to near-source strong-motion waveforms of this earthquake. We estimated source models of this earthquake in three successive period bands (5–10, 10–25, and 25–50 s) using strong-motion data and Green's functions based on a 3-D velocity structure model. The source models in the period bands of 10–25 and 25–50 s had large slips in the area to the south and southeast of the hypocenter in the depth range of 23–35 km, while the large slip area for the source model in the period band of 5–10 s was located in the deeper region ~30 km west of the hypocenter in the depth range of 35–45 km. These results indicate that long-period (10–25 and 25–50 s) and short-period (5–10 s) seismic waves were predominantly radiated from these different regions along the dip direction during the 2011 Ibaraki-oki earthquake. This along-dip variation in the dominant period of seismic radiation can be explained by the variation in scale in unstable sliding patches according to depth.

1. Introduction

To reveal the spatiotemporal heterogeneities of earthquake rupture, many earthquakes have been studied by source process analyses using seismic waveform data such as kinematic source inversion techniques (e.g., Ide, 2015; Trifunac, 1974) or back-projection techniques (Ishii et al., 2005; Kiser & Ishii, 2017). Among such studies, the spatial variation in the dominant period of seismic radiation has been discovered for interplate earthquakes (e.g., Lay et al., 2012; Yagi & Okuwaki, 2015; Yao et al., 2013), crustal earthquakes (e.g., Suzuki & Iwata, 2009; Uchide et al., 2013; Zeng et al., 1993), and intraslab earthquakes (e.g., Yin & Yao, 2016). Elucidating the spatial variation in period-dependent seismic radiation of large earthquakes is important for expanding our understanding of the generation mechanism of broadband seismic waves (e.g., Lay et al., 2012; Miyake et al., 2003; Suzuki & Iwata, 2009; Zeng et al., 1993) and the heterogeneity of physical properties on the source faults (e.g., Galvez et al., 2020; Lay et al., 2012; Yao et al., 2013). For example, Lay et al. (2012) proposed a schematic model of fault-sliding heterogeneity in subduction zones for explaining depth-varying variation in seismic radiation of large to huge interplate earthquakes including the 2004 Sumatra-Andaman earthquake, the 2010 Maule earthquake, and the 2011 Tohoku earthquake.

This paper studies the 2011 Ibaraki-oki earthquake (M_w 7.9) that occurred off the Ibaraki prefecture, Kanto, in eastern Japan at 15:15 on 11 March 2011, Japan Standard Time (JST; 06:15 on 11 March, coordinated universal time [UTC]; Figure 1). The hypocentral location and focal mechanism indicate that this event was a thrust-type interplate earthquake in the subduction zone in which the Pacific plate subducts beneath the North American plate. It was the largest aftershock of the 2011 Tohoku earthquake (M_w 9.1) and occurred ~30 min after the mainshock. Previous studies have reported on the source process of this earthquake (e.g., Honda et al., 2013; Kubo et al., 2013, 2016). However, the estimated source model differs among those studies. Kubo et al. (2013) estimated the spatiotemporal slip model of this earthquake by the kinematic source inversion of near-source strong-motion waveforms in the period band of 5–50 s and static displacements measured by GNSS. Their source model featured a large slip area ~20 km southeast of the hypocenter. On the other hand, Honda et al. (2013) investigated the seismic-wave radiation process in the short-period band of 1–10 s for this earthquake with a back-projection technique using strong-motion data and found that the

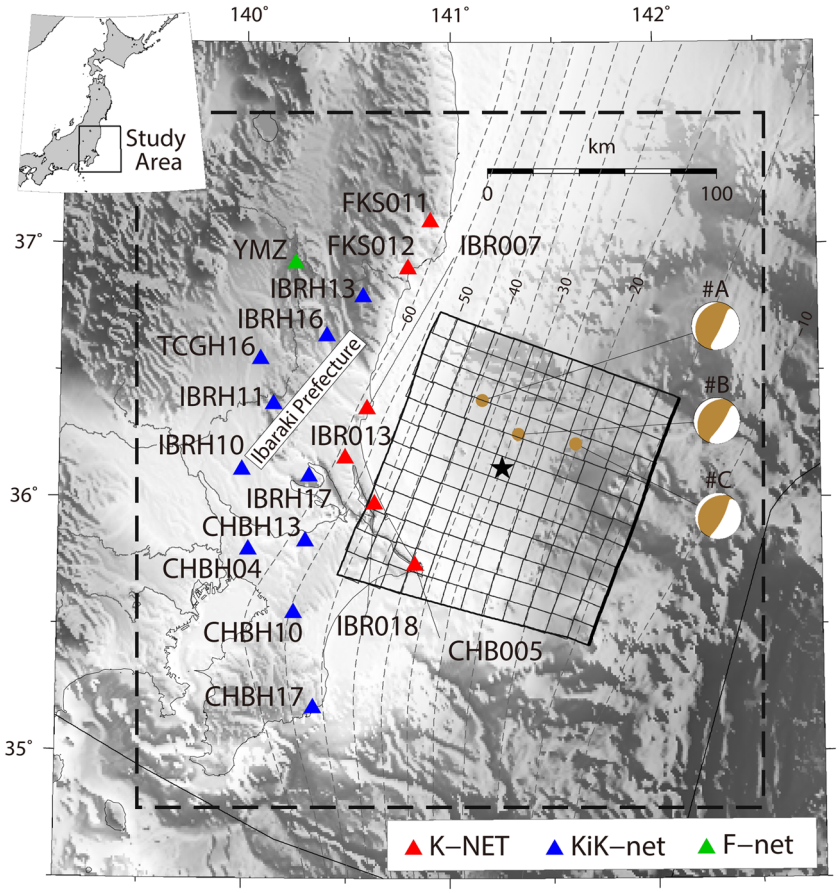

Figure 1. Map of the study area. Triangles denote the stations used in the source inversion and the color indicates the observation network: Red, blue, and green represent K-NET, KiK-net, and F-net stations, respectively. The black star represents the rupture starting point. The rectangular grid indicates the subfaults that constitute the assumed fault model. The dashed black line indicates the horizontal extent of the model space of the finite difference method for the calculation of Green's functions. The dashed gray lines indicate the isodepth contours of the plate boundary in the Japan integrated velocity structure model (JIVSM; Koketsu et al., 2012) with a 5 km interval. The earthquakes used in the waveform comparison of Figure S1 are denoted by yellow-ocher solid circles with the moment tensor solutions determined by F-net.

radiation source of the short-period seismic-waves predominantly propagated from the hypocenter to the west. The contrast in the source models between Kubo et al. (2013) and Honda et al. (2013) is expected to be due to the difference in the period range of the waveform data used in these studies. This implies the spatial variation in the dominant period of seismic radiation during the 2011 Ibaraki-oki earthquake. However, because the source models in these previous studies were estimated using different analysis methods, it is difficult to make a direct comparison between their source models and to discuss the spatial variation in period-dependent seismic radiation during the 2011 Ibaraki-oki earthquake. Thus, a unified approach must be developed to analyze the spatial variation in period-dependent seismic radiation from seismic waveform data of large earthquakes.

In this paper, we propose a multiple-period-band finite source inversion approach to reveal the spatial variation in period-dependent seismic radiation of large earthquakes, and apply it to near-source strong-motion waveforms of the 2011 Ibaraki-oki earthquake. The concept of this approach is simplified in that, first, the original waveform data for a target event is band-pass filtered in multiple successive period bands. Then, using the data set, the spatiotemporal slip model is estimated for each period band using a unified source inversion method. By comparing the source model for each period band, we are then able to discuss the spatial variation in the period-dependent seismic radiation of the 2011 Ibaraki-oki earthquake.

Previous studies (e.g., Ide, 1999; Suzuki & Iwata, 2009; Zeng et al., 1993) adopted a similar approach to that used in this study. They estimated source models in multiple-period bands for a target earthquake and discussed the spatial variation in period-dependent seismic radiation. The main difference between the previous studies and this study is that the magnitude of the target earthquakes differs as follows: $M \sim 6$ or 7 for the target events in the previous studies and $M \sim 8$ for our target event (the 2011 Ibaraki-oki earthquake). Because the 2011 Ibaraki-oki earthquake was large enough that seismic waveforms with a good signal-to-noise ratio were observed at near-source stations in period bands of up to several tens of seconds, we were able to set a longer analysis period band than those used in the previous studies. The analysis period band in the previous studies ranged from several fractions of a second to several seconds, whereas our analysis focuses on the period band of 5–50 s. Therefore, we have an opportunity to obtain an understanding of the spatial variation in period-dependent seismic radiation at longer periods. This longer analysis period band gives us another advantage in that source models in multiple period bands can be estimated using only theoretical Green's functions (GFs). Because of the difficulty in calculating appropriate theoretical waveforms for a period band shorter than 1 s, the previous studies had to use different GFs (i.e., theoretical and empirical GFs) when constructing source models in multiple-period bands. This would make it difficult to interpret the relationship between the source models in multiple-period bands because the error of theoretical GFs would differ from that of empirical GFs.

2. Multiple-Period-Band Source Inversion Approach

We estimated the source models for the 2011 Ibaraki-oki earthquake in three successive period bands (5–10, 10–25, and 25–50 s) using near-source waveform data and GFs based on a 3-D velocity structure model.

2.1. Near-Source Waveform Data

For data, we used near-source strong-motion waveforms observed by nationwide seismograph observation networks (Aoi et al., 2011; Okada et al., 2004), which are maintained by the National Research Institute for Earth Science and Disaster Resilience (NIED). These data were used because near-source data are expected to contain detailed information on fault ruptures. We used three components of the strong-motion waveforms recorded at 17 stations (Figure 1) which consist of six stations of K-NET (Aoi et al., 2011; NIED, 2019b) on the ground surface, 10 stations of KiK-net (Aoi et al., 2011; NIED, 2019b) on the ground surface, and one station of F-net (NIED, 2019a; Okada et al., 2004) in an observational vault. They are the same as the waveform data used in Kubo et al. (2016). The preprocessing of the waveform data also followed Kubo et al. (2016), except for the period band of the band-pass filter.

2.2. Green's Functions Based on 3-D Velocity Structure Model

Most previous source inversions using near-source waveform data used GFs calculated assuming 1-D stratified underground structure model (hereinafter referred to as "1-D GFs"). Recent studies adopted different 1-D structure models for each station, derived from a 3-D structure model, to consider the variation of subsurface structures among strong-motion stations (e.g., Asano & Iwata, 2009; Kubo et al., 2013). However, when the real velocity structure has a significant lateral complexity (e.g., subduction zone, large basin area), which cannot be appropriately approximated by a 1-D structure model, 1-D GFs cannot sufficiently reproduce the observed seismograms (e.g., Asano & Iwata, 2019; Graves & Wald, 2001; Kubo & Kakehi, 2013). If inadequate GFs are used in the source inversion, the model prediction error caused by the inappropriately approximated velocity structure model could be improperly forced into the solution, thus distorting the obtained source model in the source inversion. Therefore, we adopted GFs that were calculated assuming a 3-D velocity structure model (hereinafter referred to as "3-D GFs"). Graves and Wald (2001) demonstrated that in regions of complex geology, the use of well-calibrated GFs based on 3-D velocity structure can increase the resolution of the source inversion. We prepared the 3-D GFs following Kubo et al. (2016), who calculated theoretical waveforms by the 3-D FDM code, Ground Motion Simulator (Aoi et al., 2004; Aoi & Fujiwara, 1999) with a 3-D velocity structure model for Japan. For the 3-D velocity structure model, the authors used the Japan Integrated Velocity Structure Model (JIVSM) (Koketsu et al., 2012). The JIVSM was constructed to simulate long-period ground motions and to assess associated seismic hazards by modeling a regional 3-D velocity structure in Japan, simultaneously and sequentially using various kinds of data sets such as extensive refraction/reflection experiments, gravity surveys, surface geology, borehole logging data, microtremor surveys, and earthquake ground motion records

(Koketsu et al., 2009). The JIVSM is composed of 23 homogeneous layers including sedimentary layers at the top and an oceanic mantle layer at the bottom, and it is well-suited to the waveform simulation conducted in this study. The seawater layer was not included in this waveform simulation because the assumed fault model was so deep that seawater does not affect largely the simulated waveforms at onshore stations in the target period range of this study (e.g., Hatayama, 2004; Nakanishi, 1992; Petukhin et al., 2010). The group velocity of surface waves excited by seawater is slow and they will not arrive as early as the direct *S* wave at onshore stations (Nakanishi, 1992).

To validate the 3-D GFs, we compared theoretical waveforms calculated assuming a 3-D velocity structure model with observed waveforms and theoretical waveforms calculated assuming a 1-D velocity structure model for $M \sim 6$ interplate events (see Text S1 in the supporting information for details). This comparison indicated that the reproducibility of the theoretical waveforms based on the 3-D velocity structure model is better than that of the theoretical waveforms based on a 1-D velocity structure model, particularly in the period band of 5–10 s. This suggests overall that the use of 3-D GFs is preferable for source inversions of interplate earthquakes such as the 2011 Ibaraki-oki earthquake.

2.3. Source Inversion Method

To estimate spatiotemporal slip models, we used the fully Bayesian source inversion with the multiple-time-window method, proposed by Kubo et al. (2016). The source-inversion setting also followed that of Kubo et al. (2016). The authors assumed a curved fault model based on the shape of the upper boundary of the Pacific plate in the Japan Integrated Velocity Structure Model (JIVSM; Koketsu et al., 2012) and divided it into 12 rectangle subfaults along the strike direction and 12 subfaults along the dip direction (Figure 1). The subfault size was set to ~10 km × 10 km. The slip time history at each subfault was represented by a series of nine smoothed-ramp functions with 4.0 s width, each with a 2.0 s lag. The triggering velocity of the first time window was assumed to be 2.0 km/s.

The fully Bayesian inversion is expected to produce appropriate hyperparameters (Σ, A) and a plausible slip model when using a nonnegative slip constraint (Fukuda & Johnson, 2008; Kubo et al., 2016). Here, Σ and A represent logarithms of unknown scale factors for covariance matrices of errors in the observation equation and the smoothing constraint, respectively. We conducted the fully Bayesian source inversion for each period band and obtained a plausible source model in the period band of 25–50 s. However, in the period bands of 5–10 and 10–25 s, the derived slip models were more complex, and the estimated values of seismic moment were excessively large (M_w 8.5 for 5–10 s, and 8.1 for 10–25 s) compared to those from other period-band models and the Global CMT (Dziewonski et al., 1981; Ekström et al., 2012) (M_w 7.7 for 25–50 s, 7.9 for 5–50 s, and 7.9 from the Global CMT). Considering the goodness of fit of the waveforms between the 3-D theoretical and observed waveforms for $M \sim 6$ events (Figure S1), the waveform fits in these period bands were exceedingly good (variance reduction of 76.1% for 5–10 s, and 91.7% for 10–25 s). Therefore, we judged that the source inversions in the period bands of 5–10 and 10–25 s were unable to determine the appropriate values of the hyperparameters (Σ, A). This was partly caused by ignoring the model prediction errors in the observation equation in Kubo et al. (2016). The GF error, which is one of the model prediction errors, is expected to increase as the analysis period shortens (Figure S1), and this may explain why appropriate hyperparameters were not determined in the short-period band. This problem could be addressed by considering the model prediction errors of GFs in source inversions (e.g., Yagi & Fukahata, 2011). However, this requires that the determinant of the covariance matrix in the observation equation is calculated every time the unknown parameters are updated. The use of this technique together with the MCMC method, which gradually updates the unknown parameters and was adopted in Kubo et al. (2016), requires significant computation time to reach convergence in the Markov chain. Because it is difficult to consider the prediction errors at present, we used an alternative approach. In this study, we adopted the fully Bayesian source inversion where $\Sigma - A\ (= \Lambda)$ is fixed in the period bands of 5–10 and 10–25 s and conducted several inversions varying the value of Λ. The increase of Λ means that the smoothing constraint becomes weak and the waveform fit becomes better, while wasted slips are produced and the seismic moment of the obtained source model becomes large. We selected the value of Λ satisfying the following conditions: (1) The waveform fit is as good as possible and (2) the moment magnitude of the obtained solution is not larger than 7.9, which is the moment magnitude of the solution in the period band of 5–50 s (Kubo et al., 2016) or the Global CMT. The selected values of Λ in the period bands of 5–10 and 10–25 s were 0.5 and 0.0, respectively.

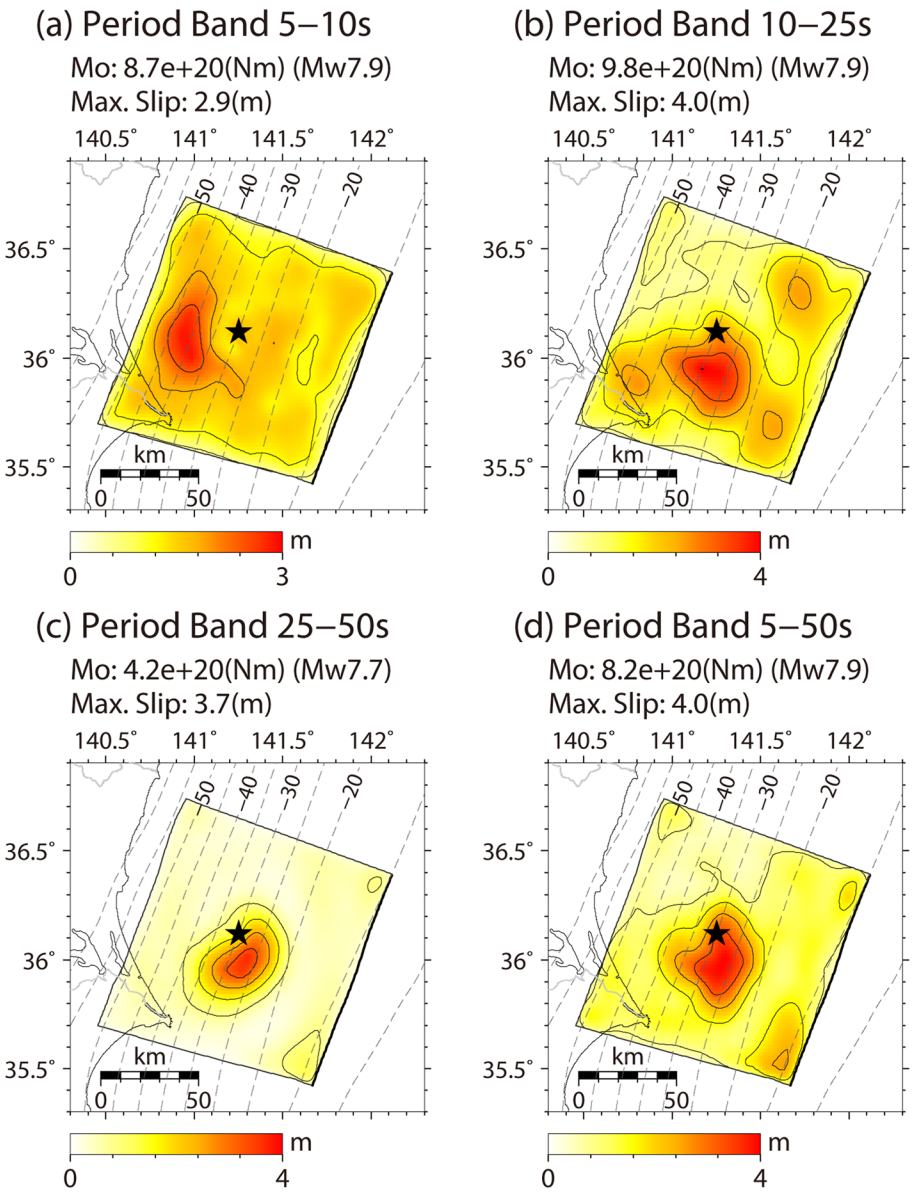

Figure 2. Slip distribution of the source models in the period bands of (a) 5–10 s, (b) 10–25 s, (c) 25–50 s, and (d) 5–50 s. solid stars indicate the epicenter and the dashed gray lines indicate the isodepth contours of the plate boundary in the JIVSM (Koketsu et al., 2012) at 5 km intervals. The source model in the period band of 5–50 s is the same as that obtained by Kubo et al. (2016).

To examine the resolution and robustness of the source inversion, we conducted synthetic tests (see Text S2 for details). The synthetic tests suggested that the source inversions in all period bands could reasonably recover the slip distribution of input models, although the maximum slip would be underestimated. Because the artifact slips are thinly distributed over the fault plane in the synthetic test in the period band of 5–10 s, the comparison of source models in different period bands hereafter is limited only to the large slip part of each source model. This test also highlights the importance of using 3-D GFs to improve the source inversion resolution for subduction earthquakes, especially in the period band of 5–10 s.

3. Results

Figure 2 shows the slip distribution for each period band with the seismic moment and maximum slip, which are also listed in Table 1. The snapshots of the rupture propagation for each period band at a time

Table 1
List of the Seismic Moment, Maximum Slip, and Variance Reduction for the Source Model in Each Period Band

Period band (s)	M_0 (nm)	M_w	Max. slip (m)	Variance reduction (%)
5–10	8.7×10^{20}	7.9	2.9	70.1
10–25	9.8×10^{20}	7.9	4.0	87.4
25–50	4.2×10^{20}	7.7	3.7	90.5
5–50[a]	8.2×10^{20}	7.9	4.0	82.4

[a]The source model in the period band of 5–50 s is the same as that obtained by Kubo et al. (2016).

step of 5 s are shown in Figure 3. In the source models in the period bands of 10–25 and 25–50 s, a large slip area was located to the south and southeast of the hypocenter in the depth range of 23–35 km. Approximately 10 s after the rupture initiation at the hypocenter, the rupture with a large slip propagated toward the south and southeast. The total rupture duration was ~25 s. Meanwhile, a large slip area for the source model in the period band of 5–10 s was located in the deep region ~30 km west of the hypocenter, in the depth range of 35–45 km. In this period band, the westward downdip rupture started ~10 s after the rupture initiation and continued for 35 s.

Figure 4a shows the source time function at each subfault of the source model in each period band. Figures 4b and 4c show the source time function at the selected subfaults. The subfault that shows a large slip in the source model in the period bands of 10–25 and 25–50 s (Figure 4b) had a significantly lower amplitude of the source time function in the source model in the period band of 5–10 s compared to those of other period band models. On the other hand, the subfault that shows a large slip in the source model in the period band of 5–10 s (Figure 4c) had a lower amplitude of the source time function in the source model in the period band of 25–50 s.

These results suggest that the 2011 Ibaraki-oki earthquake nearly simultaneously ruptured the shallow region (depth of 23–35 km) and the deep region (depth of 35–45 km). The seismic radiation characteristic of this earthquake varied along the dip direction. Long-period (10–25 and 25–50 s) seismic waves strongly radiated from the shallow region, while short-period (5–10 s) seismic waves radiated from the deep region.

Figure 5 shows a comparison of observed and synthetic waveforms for each period band and Table 1 lists the variance reduction for each period band. The waveform fit was sufficient in all period bands.

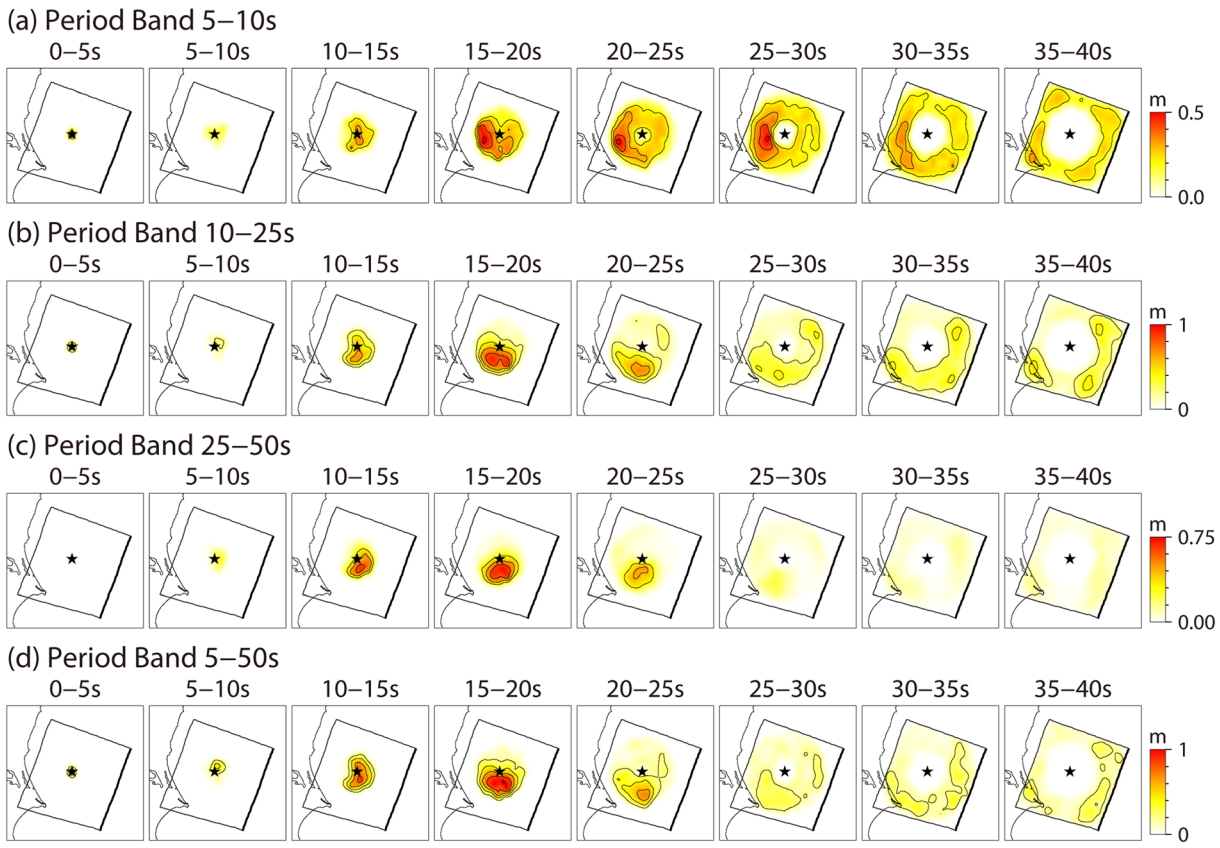

Figure 3. Snapshots of the rupture propagation for the source models in the period bands of (a) 5–10 s, (b) 10–25 s, (c) 25–50 s, and (d) 5–50s. Slip for every 5 s is shown in each panel. Solid stars indicate the epicenter. The source model in the period band of 5–50 s is the same as that obtained by Kubo et al. (2016).

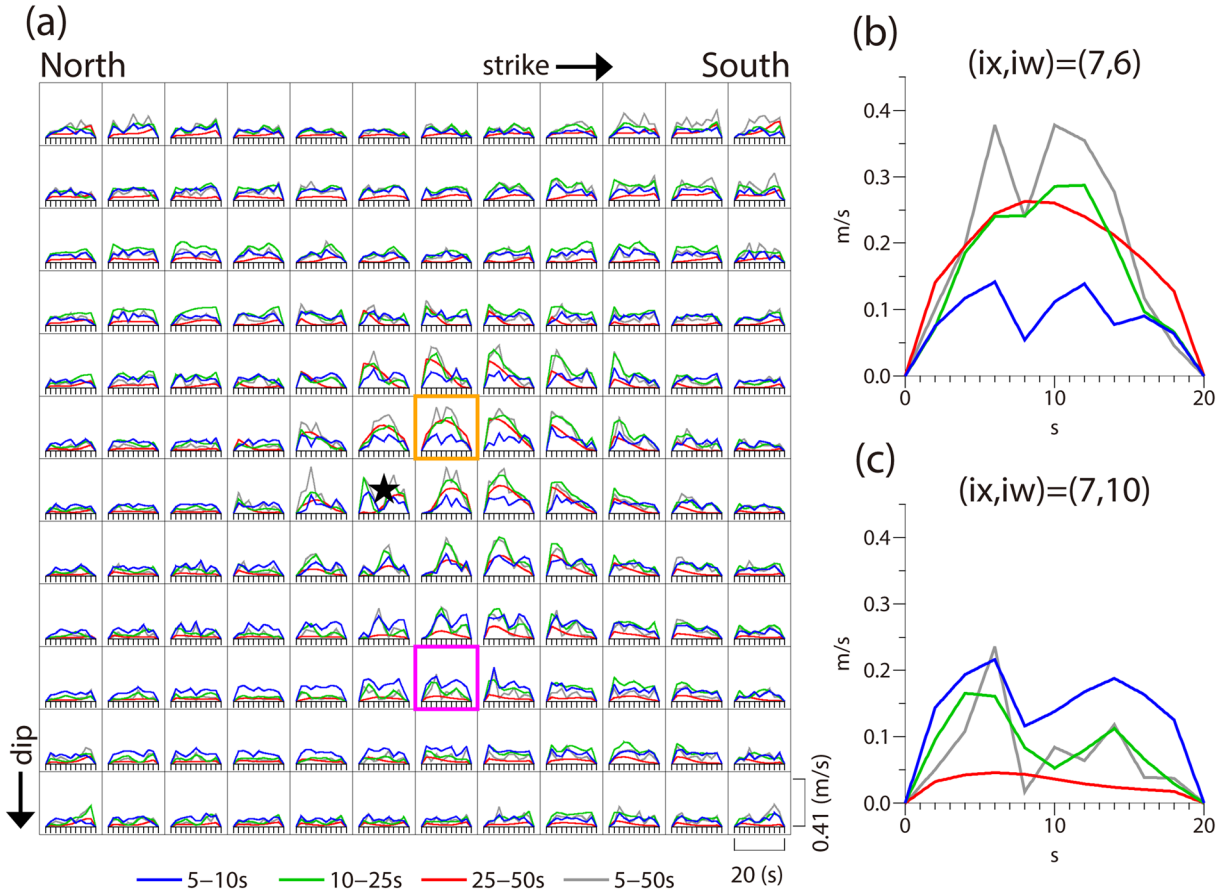

Figure 4. (a) Source time function at each subfault for the source models in the period bands of 5–10 s (blue), 10–25 s (green), 25–50 s (red), and 5–50 s (gray). The solid star indicates the subfault corresponding to the epicenter. The subfaults emphasized by orange and magenta lines correspond to the subfaults in (b) and (c), respectively. (b, c) Source time function at two selected subfaults for the source models in the period bands of 5–10 s (blue), 10–25 s (green), 25–50 s (red), and 5–50 s (gray); ix and iw are the subfault numbers along the strike and dip directions, respectively. The source model in the period band of 5–50 s is the same as that obtained by Kubo et al. (2016).

For comparison, Figures 2–4 show a source model in the period band of 5–50 s identical to the model obtained by Kubo et al. (2016), which is similar to the source model in Kubo et al. (2013). The source model in the period band of 5–50 s is similar to those in the period bands of 10–25 and 25–50 s, indicating that the source model obtained in the period band of 5–50 s strongly reflected the rupture process relating to the generation of long-period (10–50 s) waveforms. The radiation image of short-period seismic waves in the period band of 1–10 s (Honda et al., 2013) is also consistent with our source model in the period band of 5–10 s, suggesting that it is difficult to derive information on seismic-wave generation in the short-period band (5–10 s) from the source inversion results in the period band of 5–50 s. Thus, we infer that the multiple-period-band source inversion approach is useful for revealing the broadband seismic-radiation characteristics of a large earthquake.

4. Discussion

4.1. Along-Dip Variation in Period-Dependent Seismic Radiation

Lay et al. (2012) suggested the variation in earthquake rupture properties with depth in recent megathrust earthquakes, and segmented interplate faults according to depth. Domain A extends from the trench to a depth of 15 km and would experience either aseismic deformation or large coseismic displacements in tsunami earthquakes. Domain B, in the depth range of 15–35 km, is where large slip would occur with modest amounts of short-period seismic radiation. Domain C, in the depth range of 35–55 km, is where moderate slip would occur with significant coherent short-period seismic radiation. An unanswered issue

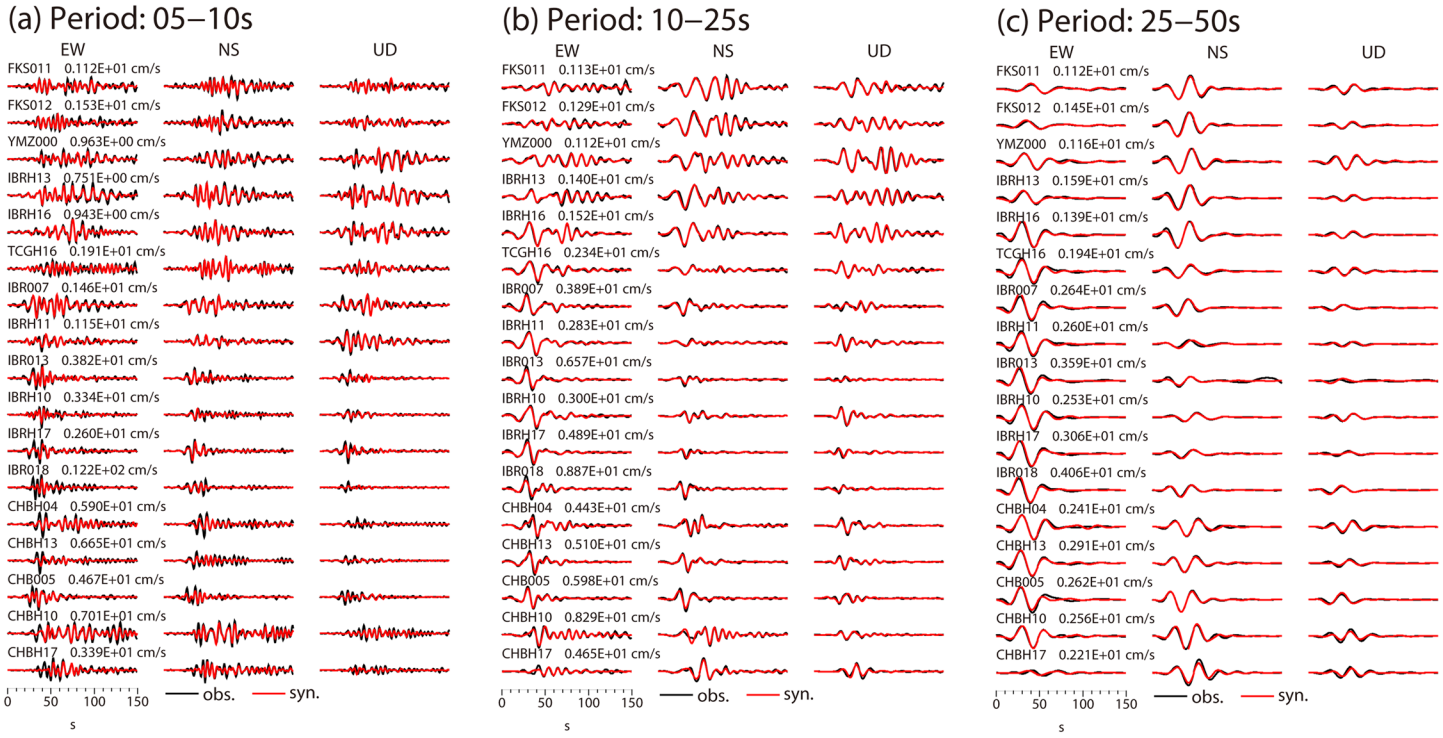

Figure 5. Comparison of observed (black) and synthetic (red) velocity waveforms in the period bands of (a) 5–10 s, (b) 10–25 s, and (c) 25–50s. The maximum values of the three-component waveforms are shown above each trace.

in Lay et al. (2012) is the border of the dominant period of seismic radiation between domains B and C. This is because the discussion in Lay et al. (2012) was mainly based on a comparison of two source models inferred from short- and long-period seismic waves: one is the back-projection result with short-period (~1 s) seismic waves and the other is the source inversion result with long-period (>10 s) seismic waveforms. Because the multiple-period-band source inversion proposed by this study can produce source models in successive period bands (5–10, 10–25, and 25–50 s), we can trace the transition of the dominant period of seismic waves radiated from each domain.

Our study demonstrates that the 2011 Ibaraki-oki earthquake had an along-dip variation in period-dependent seismic radiation: seismic waves in the period band of 10–25 and 25–50 s strongly radiated from the shallow region (depth of 23–35 km), whereas seismic waves in the period band of 5–10 s radiated from the deep region (depth of 35–45 km). These source areas are coincident with domains B and C in Lay et al. (2012), respectively. This implies that the border of the dominant period of seismic radiation between domains B and C is ~10 s, at least in the source region of the 2011 Ibaraki-oki earthquake: seismic waves at periods longer than 10 s significantly radiated from domain B, while the seismic radiation at periods shorter than 10 s was stronger in domain C.

Lay et al. (2012) suggested that the along-dip variation in seismic radiation between domains B and C would be caused by the variation in scale in unstable sliding patches and background stress with depth. Domain B would have large, uniform regions of stable sliding that could have large slips, but also generate modest amounts of short-period radiation upon failure. Domain C would have patchy, smaller-scale regions of stable sliding that could produce coherent short-period radiation on failure. It seems reasonable that the simultaneous fault rupture in domains B and C with different scales of unstable sliding patches caused the along-dip variation in the dominant period of seismic radiation during the 2011 Ibaraki-oki earthquake.

4.2. Comparison With Seismicity and Afterslips

Kubo et al. (2013) demonstrated that the seismicity of interplate earthquakes before and after the 2011 Ibaraki-oki earthquake was low in the large slip area of this earthquake. Figures 6a and 6b compare the

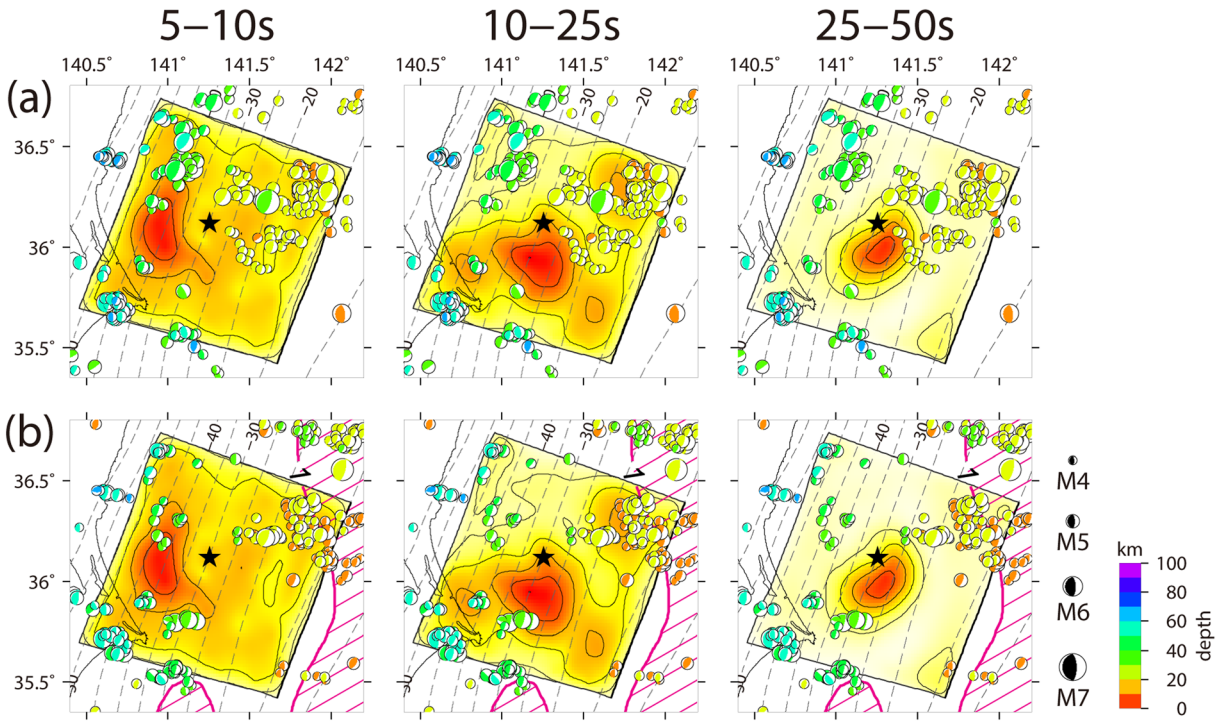

Figure 6. Map view of the source model in each period band compared with the spatial distribution of focal mechanisms of interplate earthquakes in the period of (a) 1997 to 14:46 on 11 March 2011 [JST] (before the 2011 Tohoku earthquake) and (b) 15:15 on 11 March 2011 [JST] to 2015 (after the 2011 Ibaraki-oki earthquake). These interplate earthquakes were selected from the F-net moment tensor catalog using the following conditions: 155° ≤ strike ≤ 245°, 0° ≤ dip ≤ 40°, 45° ≤ rake ≤ 135°, 10 km ≤ depth ≤ 80 km, and $M_w \geq 4$. The size of the focal mechanisms is proportional to its moment magnitude. The magenta-shaded zone in Figure 6b represents the distribution of cumulative afterslip values over 1 m for 5 years after the 2011 Tohoku earthquake (Wang et al., 2018).

estimated source model in each period band with the spatial distribution of interplate earthquakes before and after the 2011 Ibaraki-oki earthquake. The seismic activity in both periods was low in the large slip area of the source models in the period bands of 10–25 and 25–50 s, as reported in Kubo et al. (2013). Moreover, few interplate earthquakes occurred in the large slip area of the source model in the period band of 5–10 s. This implies that the interplate stress in the two large slip areas had accumulated without the stress release of interplate earthquakes and most of the accumulated interplate stress was released by the 2011 Ibaraki-oki earthquake.

Wang et al. (2018) investigated the short-term postseismic crustal deformation of the 2011 Tohoku earthquake from land and seafloor geodetic measurements accounting for viscoelastic relaxation. The authors suggested that the afterslip distribution of the 2011 Tohoku earthquake had three characteristics: a lack of significant deep afterslip downdip of the main rupture; a moderate deep afterslip slightly north of the main rupture; and a large shallow afterslip south of the main rupture. The south afterslip zone is located off the east coast of Kanto (shaded magenta zone in Figure 6b). The main afterslips of this zone were located at the updip side of the source region of the 2011 Ibaraki-oki earthquake, and their depth corresponds to domain A in the segmentation of Lay et al. (2012).

5. Conclusions

To further elucidate the broadband characteristics of seismic radiation and earthquake rupture process, we proposed an estimation approach of source models in multiple-period bands. We applied this multiple-period-band source inversion approach to the 2011 Ibaraki-oki earthquake and estimated the source models in three successive period bands (5–10, 10–25, and 25–50 s) using near-source strong-motion waveforms and 3-D GFs. We also confirmed the validity of 3-D GFs using the waveform comparison for M ~ 6

interplate events. Furthermore, the synthetic tests demonstrated that the source inversion in all period bands can reasonably recover the slip distribution of input models. The estimated rupture process in the period band of 5–10 s differed from those in the period bands of 10–25 and 25–50 s, in that the latter two featured large slips in the area south and southeast of the hypocenter, while the large slip area for the source model in the period band of 5–10 s was located in the deep region ~30 km west of the hypocenter. In the large slip area of the source model in each period band, there were few interplate earthquakes before and after the 2011 Ibaraki-oki earthquake.

Results of this study also indicate that long-period (10–25 and 25–50 s) and short-period (5–10 s) seismic waves were predominantly radiated from the shallow and deep regions, respectively, during the 2011 Ibaraki-oki earthquake. This suggests that the 2011 Ibaraki-oki earthquake had an along-dip variation in the dominant period of seismic radiation, which explains the variation in previously reported source models. The along-dip variation in period-dependent seismic radiation is consistent with the along-dip segmentation of the interplate fault suggested by Lay et al. (2012). It seems reasonable to conclude that the 2011 Ibaraki-oki earthquake almost simultaneously ruptured domains B and C, as proposed by Lay et al. (2012) and that these domains with different scales of unstable sliding patches radiated seismic waves with different dominant periods. This study also implies that the border of the dominant period of seismic radiation between domains B and C is ~10 s.

In addition to the 2011 Ibaraki-oki earthquake, large interplate earthquakes have occurred along the Japan Trench; some of which were considered to have the spatial variation in period-dependent seismic radiation as follows: the 1994 far east off Sanriku earthquake (M_w 7.9; e.g., Nakahara et al., 1998) and the 2011 Tohoku earthquake (M_w 9.1; e.g., Ide et al., 2011; Koper et al., 2011; Lay et al., 2012). However, the source models of these events also have the same issue as the 2011 Ibaraki-oki earthquake, which is that short- and long-period source models were estimated using different analysis methods, rendering direct comparisons of these source models difficult. Therefore, to better understand the spatial variation in period-dependent seismic radiation along the Japan Trench, it is important to estimate source models in multiple period bands for these events using the approach proposed in this study.

Data Availability Statement

Waveform records at K-NET, KiK-net (NIED, 2019b), and F-net (NIED, 2019a) are available at these websites (http://www.kyoshin.bosai.go.jp/ and http://www.fnet.bosai.go.jp/). The JIVSM (Koketsu et al., 2012) is available at this website (https://www.jishin.go.jp/evaluation/seismic_hazard_map/lpshm/12_choshuki_dat/). The moment tensor solution catalog of F-net is available at this website (http://www.fnet.bosai.go.jp/). The focal mechanism catalog of the Global CMT is available at this website (https://www.globalcmt.org/). The Japan Meteorological Agency unified seismic catalog is available at this website (https://www.data.jma.go.jp/svd/eqev/data/bulletin/index_e.html).

Acknowledgments

The Generic Mapping Tools (Wessel & Smith, 1998) was used to draw the figures. This study was supported by JSPS KAKENHI Grant Numbers 14J06763, 26282104, 25750146, and 17K14384, and by the Ministry of Education, Culture, Sports, Science and Technology (MEXT) of Japan, under its Earthquake and Volcano Hazards Observation and Research Program.

References

Aoi, S., & Fujiwara, H. (1999). 3-D finite difference method using discontinuous grids. *Bulletin of the Seismological Society of America*, *89*(4), 918–930.

Aoi, S., Hayakawa, T., & Fujiwara, H. (2004). Ground motion simulator: GMS. *BUTSURI-TANSA*, *57*, 651–666. (in Japanese with English abstract)

Aoi, S., Kunugi, T., Nakamura, H., & Fujiwara, H. (2011). Deployment of new strong motion seismographs of K-NET and KiK-net. In *Earthquake data in engineering seismology, geotechnical, geological, and earthquake engineering* (Vol. 14, pp. 167–186). Dordrecht, Netherlands: Springer. https://doi.org/10.1007/978-94-007-0152-6_12

Asano, K., & Iwata, T. (2009). Source rupture process of the 2004 Chuetsu, mid-Niigata prefecture, Japan, earthquake inferred from waveform inversion with dense strong-motion data. *Bulletin of the Seismological Society of America*, *99*(1), 123–140. https://doi.org/10.1785/0120080257

Asano, K., & Iwata, T. (2019). Source rupture process of the 2018 Hokkaido eastern Iburi earthquake deduced from strong-motion data considering seismic wave propagation in three-dimensional velocity structure. *Earth, Planets and Space*, *71*(1), 101. https://doi.org/10.1186/s40623-019-1080-0

Dziewonski, A. M., Chou, T.-A., & Woodhouse, J. H. (1981). Determination of earthquake source parameters from waveform data for studies of global and regional seismicity. *Journal of Geophysical Research*, *86*(B4), 2825–2852. https://doi.org/10.1029/JB086iB04p02825

Ekström, G., Nettles, M., & Dziewonski, A. M. (2012). The global CMT project 2004-2010: Centroid-moment tensors for 13,017 earthquakes. *Physics of the Earth and Planetary Interiors*, *200-201*, 1–9. https://doi.org/10.1016/j.pepi.2012.04.002

Fukuda, J., & Johnson, K. M. (2008). A fully Bayesian inversion for spatial distribution of fault slip with objective smoothing. *Bulletin of the Seismological Society of America*, *98*(3), 1128–1146. https://doi.org/10.1785/0120070194

Galvez, P., Petukhin, A., Irikura, K., & Somerville, P. (2020). Dynamic source model for the 2011 Tohoku earthquake in a wide period range combining slip reactivation with the short-period ground motion generation process. *Pure and Applied Geophysics*, *177*(5), 2143–2161. https://doi.org/10.1007/s00024-019-02210-7

Graves, R. W., & Wald, D. J. (2001). Resolution analysis of finite fault source inversion using one- and three-dimensional Green's functions 1. Strong motions. *Journal of Geophysical Research*, *106*(B5), 8767–8788. https://doi.org/10.1029/2000JB900435

Hatayama, K. (2004). *Theoretical evaluation of effects of sea on seismic ground motion*. Paper presented at the Proceedings of the 13th World Conference on Earthquake Engineering, paper no. 3229. Vancouver, Canada.

Honda, R., Yukutake, Y., Ito, H., Harada, M., Aketagawa, T., Yoshida, A., et al. (2013). Rupture process of the largest aftershock of the *M* 9 Tohoku-oki earthquake obtained from a back-projection approach using the MeSO-net data. *Earth, Planets and Space*, *65*(8), 917–921. https://doi.org/10.5047/eps.2013.01.003

Ide, S. (1999). Source process of the 1997 Yamaguchi, Japan, earthquake analyzed in different frequency bands. *Geophysical Research Letters*, *26*(13), 1973–1976. https://doi.org/10.1029/1999GL900441

Ide, S. (2015). 4.09—Slip inversion. In *Treatise on geophysics* (2nd ed., pp. 215–241). Oxford: Elsevier. https://doi.org/10.1016/B978-0-444-53802-4.00076-2

Ide, S., Baltay, A., & Beroza, G. C. (2011). Shallow dynamic overshoot and energetic deep rupture in the 2011 M_w 9.0 Tohoku-oki earthquake. *Science*, *332*(6036), 1426–1429. https://doi.org/10.1126/science.1207020

Ishii, M., Shearer, P. M., Houston, H., & Vidale, J. E. (2005). Extent, duration and speed of the 2004 Sumatra-Andaman earthquake imaged by the Hi-net array. *Nature*, *435*(7044), 933–936. https://doi.org/10.1038/nature03675

Kiser, E., & Ishii, M. (2017). Back-projection imaging of earthquakes. *Annual Review of Earth and Planetary Sciences*, *45*(1), 271–299. https://doi.org/10.1146/annurev-earth-063016-015801

Koketsu, K., Miyake, H., & Suzuki, H. (2012). *Theoretical evaluation of effects of sea on seismic ground motion*. Paper presented at the 15th World Conference on Earthquake Engineering, paper no. 1773, Lisbon, Portugal.

Koketsu, K., Miyake, H., & Tanaka, Y. (2009). A proposal for a standard procedure of modeling 3-D velocity structures and its application to the Tokyo metropolitan area, Japan. *Tectonophysics*, *472*(1–4), 290–300. https://doi.org/10.1016/j.tecto.2008.05.037

Koper, K. D., Hutko, A. R., Lay, T., Ammon, C. J., & Kanamori, H. (2011). Frequency-dependent rupture process of the 2011 M_w 9.0 Tohoku earthquake: Comparison of short-period *P* wave backprojection images and broadband seismic rupture models. *Earth, Planets and Space*, *63*(7), 599–602. https://doi.org/10.5047/eps.2011.05.026

Kubo, H., Asano, K., & Iwata, T. (2013). Source-rupture process of the 2011 Ibaraki-oki, Japan, earthquake (M_w 7.9) estimated from the joint inversion of strong-motion and GPS data: Relationship with seamount and Philippine sea plate. *Geophysical Research Letters*, *40*, 3003–3007. https://doi.org/10.1002/grl.50558

Kubo, H., Asano, K., Iwata, T., & Aoi, S. (2016). Development of fully Bayesian source waveform inversion with multi-time-window method. *Geophysical Journal International*, *204*(3), 1601–1619. https://doi.org/10.1093/gji/ggv540

Kubo, H., & Kakehi, Y. (2013). Source process of the 2011 Tohoku earthquake estimated from the joint inversion of teleseismic body waves and geodetic data including seafloor observation data: Source model with enhanced reliability by using objectively determined inversion settings. *Bulletin of the Seismological Society of America*, *103*(2B), 1195–1220. https://doi.org/10.1785/0120120113

Lay, T., Kanamori, H., Ammon, C. J., Koper, K. D., Hutko, A. R., Ye, L., et al. (2012). Depth-varying rupture properties of subduction zone megathrust faults. *Journal of Geophysical Research*, *117*, B04311. https://doi.org/10.1029/2011JB009133

Miyake, H., Iwata, T., & Irikura, K. (2003). Source characterization for broadband ground-motion simulation: Kinematic heterogeneous source model and strong motion generation area. *Bulletin of the Seismological Society of America*, *93*(6), 2531–2545. https://doi.org/10.1785/0120020183

Nakahara, H., Nishimura, T., Sato, H., & Ohtake, M. (1998). Seismogram envelope inversion for the spatial distribution of high-frequency energy radiation from the earthquake fault: Application to the 1994 far east off Sanriku earthquake, Japan. *Journal of Geophysical Research*, *103*(B1), 855–867. https://doi.org/10.1029/97JB02676

Nakanishi, I. (1992). Rayleigh waves guided by sea-trench topography. *Geophysical Research Letters*, *19*, 2385–2388. https://doi.org/10.1029/92GL02438

National Research Institute for Earth Science and Disaster Resilience (2019a) NIED F-net. National Research Institute for Earth Science and Disaster Resilience. https://doi.org/10.17598/NIED.0005

National Research Institute for Earth Science and Disaster Resilience (2019b) NIED K-NET, KiK-net. National Research Institute for Earth Science and Disaster Resilience. https://doi.org/10.17598/NIED.0004

Okada, Y., Kasahara, K., Hori, S., Obara, K., Sekiguchi, S., Fujiwara, H., & Yamamoto, A. (2004). Recent progress of seismic observation networks in Japan —Hi-net, F-net, K-net and KiK-net—. *Earth, Planets and Space*, *56*(8), xv–xxviii. https://doi.org/10.1186/BF03353076

Petukhin, A., Iwata, T., & Kagawa, T. (2010). Study on the effect of the oceanic water layer on strong ground motion simulations. *Earth, Planets and Space*, *62*(8), 621–630. https://doi.org/10.5047/eps.2010.07.014

Suzuki, W., & Iwata, T. (2009). Broadband seismic wave radiation process of the 2000 Western Tottori, Japan, earthquake revealed from wavelet domain inversion. *Journal of Geophysical Research*, *114*(B8), B08302. https://doi.org/10.1029/2008JB006130

Trifunac, M. D. (1974). A three-dimensional dislocation model for the San Fernando, California, earthquake of February 9, 1971. *Bulletin of the Seismological Society of America*, *64*(1), 149–172.

Uchide, T., Yao, H., & Shearer, P. M. (2013). Spatio-temporal distribution of fault slip and high-frequency radiation of the 2010 El Mayor-Cucapah, Mexico earthquake. *Journal of Geophysical Research: Solid Earth*, *118*, 1546–1555. https://doi.org/10.1002/jgrb.50144

Wang, K., Sun, T., Brown, L., Hino, R., Tomita, F., Kido, M., et al. (2018). Learning from crustal deformation associated with the *M*9 2011 Tohoku-oki earthquake. *Geosphere*, *14*(2), 552–571. https://doi.org/10.1130/GES01531.1

Wessel, P., & Smith, W. H. F. (1998). New, improved version of generic mapping tools released. *Eos Transactions AGU*, *79*(47), 579. https://doi.org/10.1029/98EO00426

Yagi, Y., & Fukahata, Y. (2011). Introduction of uncertainty of Green's function into waveform inversion for seismic source processes. *Geophysical Journal International*, *186*(2), 711–720. https://doi.org/10.1111/j.1365-246X.2011.05043.x

Yagi, Y., & Okuwaki, R. (2015). Integrated seismic source model of the 2015 Gorkha, Nepal, earthquake. *Geophysical Research Letters*, *42*, 6229–6235. https://doi.org/10.1002/2015GL064995

Yao, H., Shearer, P. M., & Gerstoft, P. (2013). Compressive sensing of frequency-dependent seismic radiation from subduction zone megathrust ruptures. *Proceedings of the National Academy of Sciences*, *110*(12), 4512–4517. https://doi.org/10.1073/pnas.1212790110

Yin, J., & Yao, H. (2016). Rupture and frequency-dependent seismic radiation of the 2012 *Mw* 8.6. *Sumatra strike-slip earthquake, Geophysical Journal International*, *205*(3), 1682–1693. https://doi.org/10.1093/gji/ggw105

Zeng, Y., Aki, K., & Teng, T. (1993). Mapping of the high-frequency source radiation for the Loma Prieta earthquake, California. *Journal of Geophysical Research*, *98*(B7), 11,981–11,993. https://doi.org/10.1029/93JB00346

References From the Supporting Information

Bouchon, M. (1981). A simple method to calculate Green's function for elastic layered media. *Bulletin of the Seismological Society of America*, *71*(4), 959–971.

Fukuyama, E., Ishida, M., Dreger, D. S., & Kawai, H. (1998). Automated seismic moment tensor determination by using on-line broadband seismic waveforms. *Journal of the Seismological Society of Japan (Zisin 2)*, *51*(1), 149–156 (in Japanese with English abstract). https://doi.org/10.4294/zisin1948.51.1_149

Kennett, B. L. N., & Kerry, N. J. (1979). Seismic waves in a stratified half space. *Geophysical Journal of the Royal Astronomical Society*, *57*(3), 557–583. https://doi.org/10.1111/j.1365-246X.1979.tb06779.x